Terahertz lens made out of natural stone

Daehoon Han,[1] Kanghee Lee,[1,2] Jongseok Lim,[1] Sei Sun Hong,[3] Young Kie Kim,[4] and Jaewook Ahn[1,*]

[1]Department of Physics, KAIST, Daejeon 305-701, South Korea

[2]Currently at Department of Mechanical Engineering, KAIST, Daejeon 305-701, South Korea

[3]Korea Institute of Geoscience and Mineral Resources, Daejeon 305-350, South Korea

[4]KS Photonics, Daejeon 305-701, South Korea

*Corresponding author: jwahn@kaist.ac.kr

Received 10 October 2013; revised 20 November 2013; accepted 20 November 2013; posted 20 November 2013 (Doc. ID 199213); published 13 December 2013

Terahertz (THz) time-domain spectroscopy probes the optical properties of naturally occurring solid aggregates of minerals, or stones, in the THz frequency range. Refractive index and extinction coefficient measurement reveals that most natural stones, including mudstone, sandstone, granite, tuff, gneiss, diorite, slate, marble, and dolomite, are fairly transparent for THz frequency waves. Dolomite in particular exhibits a nearly uniform refractive index of 2.7 over the broad frequency range from 0.1 to 1 THz. The high index of refraction allows flexibility in lens designing with a shorter accessible focal length or a thinner lens with a given focal length. Good agreement between the experiment and calculation for the THz beam profile confirms that dolomite has high homogeneity as a lens material, suggesting the possibility of using natural stones for THz optical elements.

OCIS codes: (080.3630) Lenses; (300.6495) Spectroscopy, terahertz; (220.4610) Optical fabrication.
http://dx.doi.org/10.1364/AO.52.008670

1. Introduction

Science and technology involved with terahertz (THz) frequency waves has become one of the most active areas of research during the past two decades [1]. THz frequency waves are located in the frequency range 0.1–10 THz (30–3000 μm in wavelength) between microwave and far-infrared (FIR) electromagnetic waves. Various research in the THz frequency range has been enabled through the development of generation and detection methods, as well as spectroscopic methods, using these waves. One of the important aspects of THz waves in material characterization application, in contrast to measurements with other light sources such as x ray or FIR waves, is the direct field amplitude measurement in THz time-domain spectroscopy (THz-TDS). Both the amplitude and phase information of a sample can be obtained simultaneously through THz-TDS, without resorting to a complex analysis [2]. Previous studies demonstrated the powerful spectroscopic capability of THz-TDS in characterizing many materials, including polymers [3], explosive materials [4], solid-state materials [5,6], chemical compounds in liquids [7], ions [8], biomaterials [9], and even the material phase transitions [10].

Recently, there have been enormous efforts devoted to the fabrication of THz optical components [11–18]. Among the THz components, lenses and off-axis parabolic mirrors play a crucial role in THz-TDS systems, which are the basic optical elements for focusing and collimating THz waves. For example, planoconvex lenses are commonly used in THz-TDS systems of linear configuration [11]. The lenses operating in the THz frequency range are fabricated with various materials: high resistive silicon [12,13], polytetrafluoroethylene (PTFE,

1559-128X/13/368670-06$15.00/0

Teflon) [3,12–14], high-density polyethylene (HDPE) [3,11,14], TPX [13], TOPAS [13,14], Zeonex [15], Picarin [16], micropowders [17], and polymeric compounds [18]. Also, special lenses such as off-axis metallic diffractive lens [19], diffractive paper lens [20], variable-focus lens using medical white oil [21], and THz Brewster lens [22] have also been reported recently.

In this paper, we demonstrate a THz lens made out of natural dolomite stone. For this, we first investigate various natural stones using THz-TDS to determine their optical constants such as refraction index and absorption coefficient. The optical constants of a limited set of stones were studied previously in the THz frequency range [23–25], but most stones from nature are yet to be studied. In this study, we investigate mudstone, sandstone, tuff, diorite, marble, granite, gneiss, slate, and dolomite. While these stones are opaque in the optical frequency range, the result of this study reveals that they are mostly transparent in the frequency range from 0.2 to 1 THz. Some natural stones, in particular, dolomite, exhibited a rather flat and high index of refraction throughout the measured THz frequency range. Note that materials with a high refractive index allow lens fabrication with more flexibility, suggesting that dolomite can be considered as a material for THz lens fabrication.

The contents of this paper are organized as follows: after we explain briefly the THz transmission measurement of natural stones in a conventional THz-TDS setup, we describe the extraction process for the complex refractive index from the stones investigated. The fabrication procedure for a THz lens using dolomite is then explained. The results of focused intensity profile measurement of the fabricated dolomite lens with respect to selective frequencies are then presented, followed by the conclusion.

2. Measurement of Optical Constants of Natural Stones

A. Experimental Procedure

For experimental measurement of the refractive index and extinction coefficient of various natural stones, we used a conventional THz-TDS setup [6]. THz waves were generated from a large-area photoconductive antenna (PCA) [26] illuminated by ultrafast optical pulses that were temporally 100 fs short, wavelength-centered at 840 nm, and produced from a mode-locked Ti:sapphire laser oscillator operating at 80 MHz repetition rate. When a THz pulse was guided by four off-axis parabolic mirrors through the sample located at the focus, another ultrafast optical pulse that was split off before the PCA and time-delayed by a linear translation stage probed the electric field profile of the THz wave as a function of the time delay via optical gating [13]. The temporal THz signals with and without the sample were separately measured via electro-optic (EO) sampling [27,28], where the polarization rotation of the probe pulse through a (110)-oriented ZnTe EO crystal with a thickness of 2 mm was mapped after a quarter-wave plate and a Wollaston prism by a pair of balanced photodiodes. By varying the time delay of the probe beam with respect to the THz pulse, the temporal electric field waveform of the THz pulse was recorded. To obtain accurate spectral information, we took a long-time-window measurement of up to 200 ps, which corresponded to the spectral resolution of 5 GHz, with a temporal step size of 100 fs. The whole THz-TDS setup was purged with dry air to reduce absorption by water vapor in the THz frequency range [29,30].

B. Retrieval of Refractive Index and Extinction Coefficient

Waveform measurement in THz-TDS allows one to obtain not only the spectral amplitude but also the spectral phase information by simply applying Fourier transformation to the time domain signal. THz-TDS directly measures the electric field, whereas conventional infrared spectroscopy such as Fourier transform infrared spectroscopy measures intensity [31], so the spectral phase information is obtained without resorting to Kramers–Kronig relationship. The THz electric field transmitted out from the sample is given as a sum of successive transmitted and reflected electric fields at both sides of the sample, which is often referred to as Fabry–Pérot etalon signal. If we denote air and the sample by subscripts 1 and 2, respectively, then the transmission $\hat{T}(\omega)$ of the sample with thickness l, which is separately measured in the experiment, is given by

$$\begin{aligned}\hat{T}(\omega) &= t_{21}t_{12}e^{i\frac{\omega}{c}(\tilde{n}_s(\omega)-n_a)l}\left\{1+\sum_{j=1}^{\delta}[r_{21}e^{i\frac{\omega}{c}\tilde{n}_s(\omega)l}]^{2j}\right\}\\ &= \rho(\omega)e^{i\Delta\phi(\omega)}\{\mathrm{FP}(\omega)\},\end{aligned} \tag{1}$$

where $\tilde{n}_s = n_s + i\kappa_s$ and n_a are the complex indices of refraction of the sample and air, respectively; δ is the number of echoes of a THz signal; ρ is the transmission amplitude; and $\Delta\phi$ is the spectral phase difference between the THz signals with and without the sample, or simply, the transmission phase. Also, t_{ij} and r_{ij} are the Fresnel coefficients given by $t_{ij} = 2\tilde{n}_i/(\tilde{n}_i+\tilde{n}_j)$ and $r_{ij} = (\tilde{n}_j-\tilde{n}_i)/(\tilde{n}_j+\tilde{n}_i)$, and $\mathrm{FP}(\omega)$ is the Fabry–Pérot term. By comparing the real and imaginary parts of the right-hand side of Eq. (1), the full expression for the complex index of refraction of the sample becomes

$$\begin{aligned}n_s &= n_a + \frac{c}{\omega l}\left(\Delta\phi - \tan^{-1}\frac{\kappa_s}{n_s} + 2\tan^{-1}\frac{\kappa_s}{n_s+n_a}\right)\\ \kappa_s &= \frac{c}{\omega l}\left(\log\frac{4n_a\sqrt{n_s^2+\kappa_s^2}}{(n_s+n_a)^2+\kappa_s^2} - \log\rho\right).\end{aligned} \tag{2}$$

For retrieval of refractive index and extinction coefficient, we used the fixed-point iteration method

[32,33], in which the initial values of the complex index of refraction were chosen in the fixed-point iteration as $t_{ij} = 1$, given by $n_s = n_a + (c/\omega l)\Delta\phi$, $\kappa_s = -(c/\omega l)\log\rho$. From the imaginary part of the complex refractive index, we can obtain the extinction coefficient as

$$\alpha(\omega) = \frac{2\omega}{c}\kappa_s(\omega). \tag{3}$$

C. Optical Constants of Stones

We measured the optical constants of nine different types of natural stones: slate, gneiss, and marble in metamorphic rocks; mudstone, sandstone, and dolomite in sedimentary rocks; and granite, tuff, and diorite in igneous rocks [34]. The samples were provided by Korea Institute of Geoscience and Mineral Resources (http://www.kigam.re.kr). Figure 1 shows the refractive indices and extinction coefficients of the investigated stones extracted by the aforementioned method in Section 2.B. Table 1 lists the typical values of refractive index n and extinction coefficient α, both measured at a frequency of 0.5 THz, along with sample thickness that varied from 6.8 to 9.4 mm. The flat lateral size of the stone samples was about 2 cm × 2 cm.

All the stones show rather flat behavior of the refractive index and a low extinction coefficient below 20 cm^{-1} over the measured frequency range from 0.2–1.2 THz.

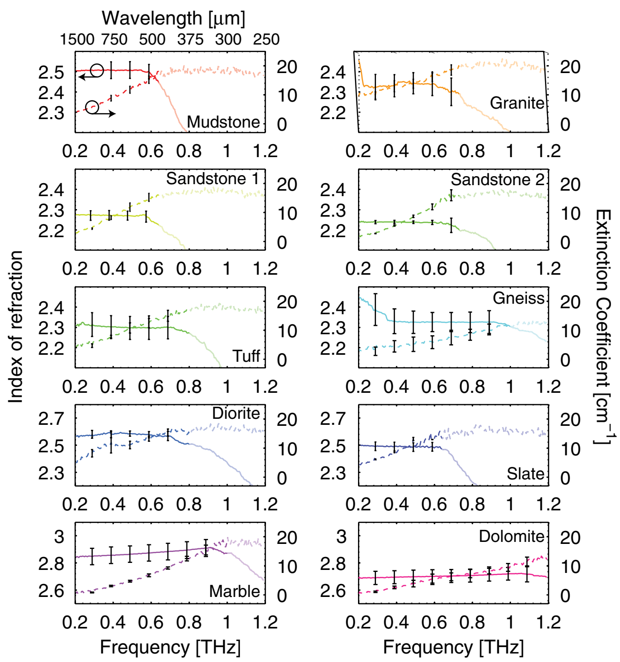

Fig. 1. Measured refractive indices and extinction coefficients of the stones in the frequency range from 0.2 to 1.2 THz corresponding to wavelength from 1500 to 250 µm. The solid lines and the dashed lines represent the extracted refractive indices and extinction coefficients, respectively, of the stones investigated.

Table 1. Refractive Indices n, Extinction Coefficients α (cm^{-1}), and Thicknesses (mm) of the Investigated Natural Stones at a Frequency of 0.5 THz

Materials	n	α	Thickness
Metamorphic rock			
Slate	2.48(3)	10.8(2)	8.65
Gneiss	2.32(5)	6.(4)	9.40
Marble	2.87(6)	5.0(3)	6.81
Sedimentary rock			
Mudstone	2.50(4)	13.(2)	8.62
Sandstone 1	2.27(2)	12.8(8)	8.95
Sandstone 2	2.24(1)	9.1(4)	9.22
Dolomite	2.70(5)	4.(1)	8.31
Igneous rock			
Granite	2.34(5)	14.(2)	7.48
Tuff	2.30(6)	11.(2)	8.41
Diorite	2.58(2)	12.(2)	8.01

3. Lens Fabrication using Dolomite

Dolomite, in particular, among the stones investigated shows low absorption and a nearly uniform refractive index of 2.7 over the measured THz frequency range. Compared with Teflon, which is widely used for THz lenses, dolomite has a higher index of refraction (see Table 2). Note that a material with a high refractive index allows more flexibility in designing a lens with a shorter accessible focal length, or a thinner lens for a given focal length. The index of refraction of dolomite is equivalent to that of silicon used commercially for semi-hemispherical THz lenses.

We designed a planoconvex lens with dolomite using the lens maker's formula [31]. When a collimated incident wave is assumed, the radius of curvature is given by

$$R = (n - 1)f, \tag{4}$$

where R, n, and f indicate the radius of curvature, the refractive index of the lens material, and the expected focal length of the lens, respectively. It is advantageous to use a material satisfying $(n - 1) > 1$ in Eq. (4) because the focal length of the lens is shorter than the radius of curvature, as shown in Fig. 2(a). We used a commercial polishing plate with radius of curvature $R = 16.19$ cm for the convex surface, which gave the expected focal length of $f = 95.2$ mm for dolomite since the refractive index of dolomite at 0.5 THz was $n = 2.70$.

We fabricated the dolomite lens by following the conventional lens-making procedure, which is

Table 2. Refractive Indices n and Extinction Coefficients α (cm^{-1}) of Dolomite and Typical Lens Materials Measured at 0.5 THz

Materials	n	α	References
Teflon (PTFE)	1.42	0.178	[3,12–14]
HDPE	1.534	2.172	[3,14]
Dolomite	2.70(5)	4.(1)	This work
Silicon	3.41	0.46	[12,13]

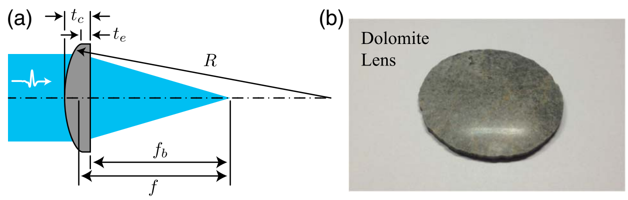

Fig. 2. (a) Specification of the fabricated dolomite lens. $f =$ effective focal length, $f_b =$ back focal length, $t_c =$ center thickness, $t_e =$ edge thickness, $R =$ radius of curvature. (b) Photo of the fabricated dolomite lens.

described, for example, in [35]. A brief description is given here. First, the bulk dolomite stone was cut into a hexahedron of size 50.2 mm × 50.2 mm × 5 mm using a diamond wheel cutter and the dolomite block was shaped into a cylindrical blank by cutting the side with a grinding machine. Both faces were then ground into typical lens shapes, one face with a spherical curvature and the other with a flat surface, by rubbing the dolomite blank on a rotating polishing plate (a concave polishing plate with a radius of curvature of 16.19 cm and a flat plate for each faces) covered with silicon carbide (SiC) micropowders of 300 mesh number compounded with water until the painted surface vanishes. And then, SiC powders of 600 and 1200 mesh numbers were sequentially used to smoothly grind the surfaces. After the grinding process, a polishing film (3M 261X Imperial Lapping film, 3 μm grade) doped with aluminium oxide (Al_2O_3) was employed to roughly polish the smoothed surface of the dolomite. Then, fine-polishing with cerium oxide (CeO_2) abrasive composed of 1 μm size powder followed.

After fine-polishing, the expected surface quality of our dolomite lens in the THz frequency range is over $\lambda/1000$. The radius of curvature of our dolomite lens is 16.19 cm, which is the same as that of the polishing plate; the thickness of the lens at the center, t_c, and at the edge, t_e, is measured to be 4.1 and 2.1 mm, respectively, and the difference between t_c and t_e is the calculated value (1.958 mm) concerning the radius of the lens. So, the expected focal length, f, is estimated to be 95.2 mm, as mentioned previously, and the back focal length, f_b, is 93.1 mm. All the parameters of the lens are shown graphically in Fig. 2(a) along with the actual photo of the fabricated lens in Fig. 2(b).

4. Results and Discussion

The shape of the focused THz field was examined by field profile measurement with the THz-TDS setup in a linear configuration as depicted in Fig. 3(a), and the photo of the setup is shown in Fig. 3(b). In this configuration, the diverging THz wave generated from the PCA was collimated by a Teflon lens with a focal length of 10 cm and focused by the dolomite lens. Then, the THz pulse and the probe laser pulse were merged by an ITO wafer and the THz signal was detected by the ZnTe crystal. We determined the focal point of the dolomite lens to be the point of maximum measured THz signal by scanning the spatial amplitude with an xyz translation stage. The field profile of the dolomite lens was obtained by two-dimensional (2D) area scanning of 9 cm × 9 cm with an interval of 300 μm. At each point in the measured 2D area, temporal profile measurement over a 10 ps time window was carried out. The maximum THz signal in the center pixel of the 2D area and the corresponding spectral amplitude obtained by the Fourier transform are shown in Fig. 3(c).

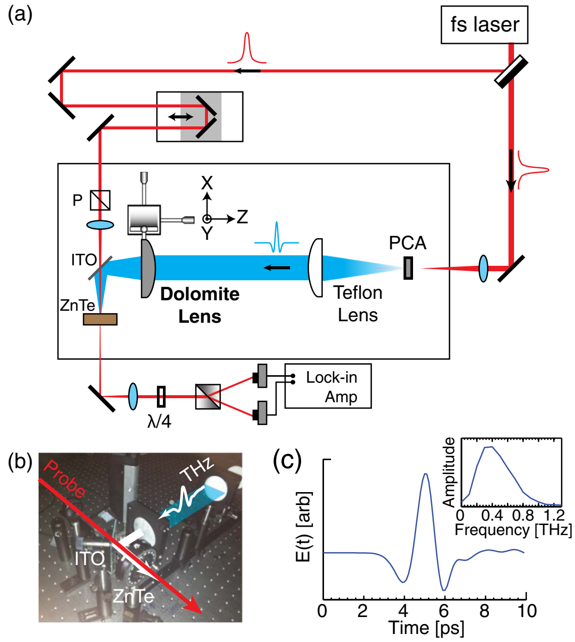

Fig. 3. (a) Schematic of our linear configuration THz-TDS setup using two THz lenses: a Teflon lens and the fabricated dolomite lens. The overall intensity profiles were measured by moving the lens with an xyz translation stage. (b) Photo of the THz-TDS setup corresponding to the boxed area in (a). The THz field is focused on to ZnTe by the fabricated dolomite lens, and ITO, playing the role of a dichroic polarization beam splitter, reflects the THz field and transmits the probe beam. (c) Temporal THz amplitude signal measured at the focal point and the corresponding amplitude spectrum after Fourier transformation.

The experimental measurement geometry of the beam profile in Fig. 4(a) is theoretically equivalent to the measurement of the Fraunhofer diffraction pattern from a circular aperture. The dolomite lens and the Teflon lens have the same diameter of 2 inches. The second lens, here the dolomite lens, yields the size of the aperture in the Fraunhofer diffraction. This lens crops the THz waves reaching the lens and only a circular segment propagates through the lens and forms the diffraction pattern in the focal plane [36]. The THz pulse in our experimental condition has a broadband spectrum and therefore, the performance of the dolomite lens can be confirmed by analyzing the beam profiles for various frequencies. We fit our amplitude profile $E(r)$, where r is the radial distance on the focal plane, to the Bessel pattern [36] given by

$$E(r) = E(0)\left|\frac{2J_1(kW_0r/2f)}{kW_0r/2f}\right|, \tag{5}$$

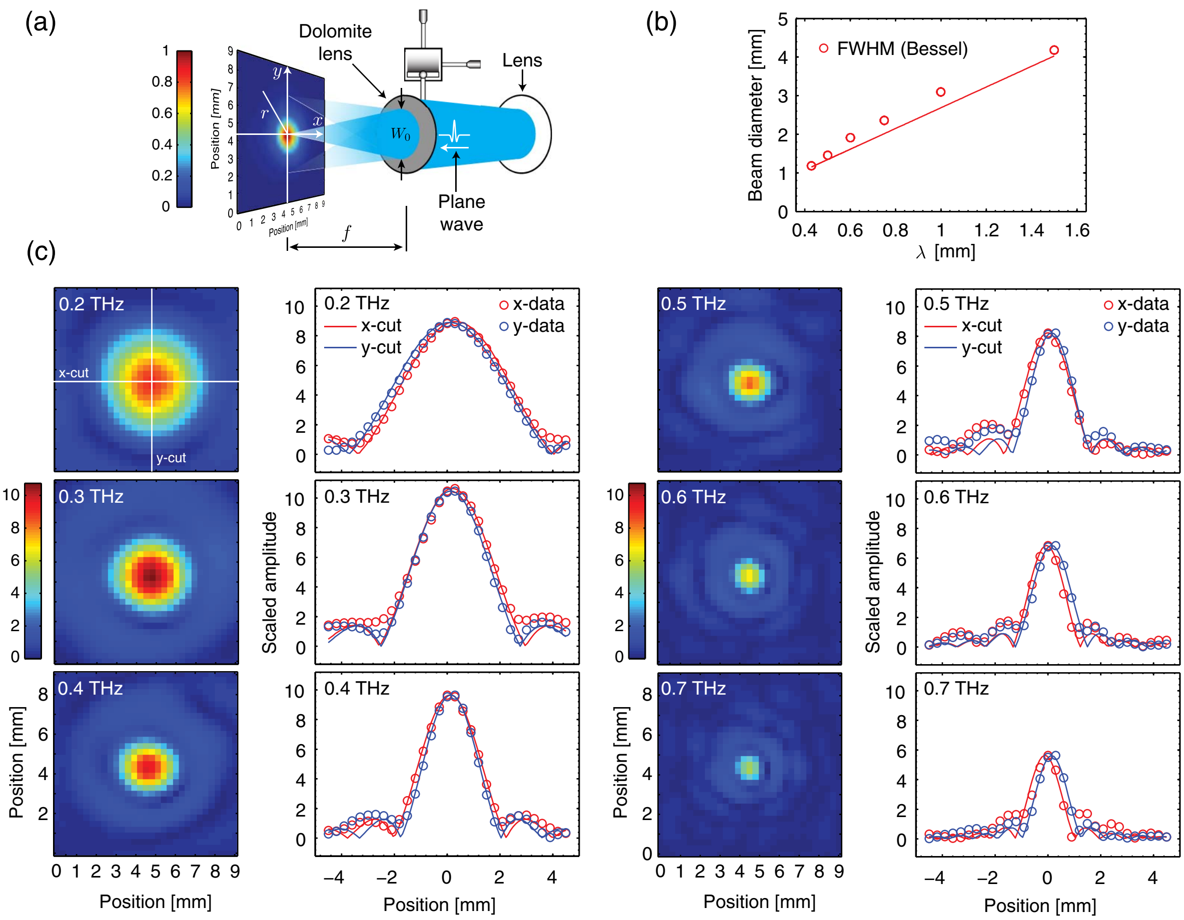

Fig. 4. (a) Beam profile measurement geometry, where W_0 in Eq. (5) is the diameter of the collimated beam. (b) Extracted diameters (FWHM) of the focused THz field at various wavelengths obtained from numerical fit of the amplitude profile to Bessel function. (c) Transmission amplitude images with respect to frequency. All amplitudes were divided by the amplitude of the THz signal without the fabricated dolomite lens. The colorbar indicates degree of magnitude compared with the THz signal without the dolomite lens. The Bessel function fitting lines (solid line) of horizontal and vertical directions across the THz amplitude profile from data (open circle) are indicated in the figures of scaled amplitude versus position with respect to frequency.

where J_1 is the first kind Bessel function of order one, k is wavenumber, f (95.2 mm) is the focal length of the lens, and W_0 is the diameter of the lens.

Figure 4(b) summarizes the extracted diameters (FWHM) of the focused THz field as a function of wavelength obtained from the numerical fit of the amplitude profiles to the Bessel pattern in Eq. (5). The measured THz beam amplitude profiles at various frequencies, and the corresponding x- and y-cross sections of the profiles are shown in Fig. 4(c). The amplitude profiles were scaled by the THz signal amplitude without the dolomite lens, and the corresponding ratio, N_{ij}, is given by

$$N_{ij}(\omega_k) = \left| \frac{E_{ij}(\omega_k)}{E_{\text{no lens}}(\omega_k)} \right|, \tag{6}$$

where $|E_{ij}(\omega_k)|$ and $|E_{\text{no lens}}(\omega_k)|$ are the amplitudes of the THz signals with and without the fabricated dolomite lens, respectively. The amplitude attenuation increases as a function of frequency as shown in Fig. 4(c). Nevertheless, the experimental result agrees well with the calculation of the THz beam profile. This result verifies that dolomite has high homogeneity as a lens material, although it shows slightly higher absorption than other lens materials.

As expected, the beam diameters show decreasing behavior as frequency increases, and are compared with the theoretical line calculated using the focal length of $f = 95.2$ mm and lens diameter of $W_0 = 50$ mm (maximal f-number $= 1.9$). The theoretical line is calculated (FWHM), $W(\lambda)$, from the Bessel pattern in Eq. (5) as

$$W(\lambda) = \frac{4.43 f}{\pi W_0} \lambda. \tag{7}$$

The good agreement between the experiment and the calculation again confirms that the fabricated lens made out of dolomite shows good performance in the THz frequency range.

5. Conclusion

In summary, we have described the use of natural stones as an optical element material in the THz frequency range. For this, we measured the optical constants of various stones from nature using THz-TDS, and, among the stones investigated, dolomite in particular exhibited a flat refractive index and low absorption over the measured THz frequency range. We fabricated a domolite planoconvex lens using the conventional lens-making procedure. The measured focused beam profiles were well explained by far-field diffraction theory in the THz frequency range. With the proof-of-principle demonstration of a THz lens made out of dolomite, we suggest the possibility of using natural stones for THz optical elements from scientific and economic aspects.

This research was supported in part by Basic Science Research Programs (2013R1A2A2A05005187, 2009-0093428) and in part by the WCI Program (WCI 2011-001) through the National Research Foundation of Korea.

References

1. M. Tonouchi, "Cutting-edge terahertz technology," Nat. Photonics **1**, 97–105 (2007).
2. W. L. Chan, J. Deibel, and D. M. Mittleman, "Imaging with terahertz radiation," Rep. Prog. Phys. **70**, 1325–1379 (2007).
3. Y.-S. Jin, G.-J. Kim, and S.-G. Jeon, "Terahertz dielectric properties of polymers," J. Korean Phys. Soc. **49**, 513–517 (2006).
4. J. Chen, Y. Chen, H. Zhao, G. J. Bastiaans, and X.-C. Zhang, "Absorption coefficients of selected explosives and related compounds in the range of 0.1–2.8 THz," Opt. Express **15**, 12060–12067 (2007).
5. Y. Kim, J. Ahn, B. G. Kim, and D.-S. Yee, "Terahertz birefringence in zinc oxide," Jpn. J. Appl. Phys. **50**, 030203 (2011).
6. M. Naftaly and R. E. Miles, "Terahertz time-domain spectroscopy: a new tool for the study of glasses in the far infrared," J. Non-Cryst. Solids **351**, 3341–3346 (2005).
7. D. S. Venables and C. A. Schmuttenmaer, "Far-infrared spectra and associated dynamics in acetonitrile-water mixtures measured with femtosecond THz pulse spectroscopy," J. Chem. Phys. **108**, 4935–4944 (1998).
8. K. J. Tielrooij, N. Garcia-Araez, M. Bonn, and H. J. Bakker, "Cooperativity in ion hydration," Science **328**, 1006–1009 (2010).
9. J.-H. Son, "Terahertz electromagnetic interactions with biological matter and their applications," J. Appl. Phys. **105**, 102033 (2009).
10. S. Wietzke, C. Jansen, T. Jung, M. Reuter, B. Baudrit, M. Bastian, S. Chatterjee, and M. Koch, "Terahertz time-domain spectroscopy as a tool to monitor the glass transition in polymers," Opt. Express **17**, 19006–19014 (2009).
11. N. Krumbholz, T. Hochreina, N. Viewega, T. Hasek, K. Kretschmer, M. Bastian, M. Mikulics, and M. Koch, "Monitoring polymeric compounding processes inline with THz time-domain spectroscopy," Polym. Test. **28**, 30–35 (2009).
12. S. Gorenflo, "A comprehensive study of macromolecules in composites using broadband terahertz spectroscopy," Ph.D. thesis (University of Freiburg, 2006).
13. B. M. Fischer, "Broadband THz time-domain spectroscopy of biomolecules: a comprehensive study of the dielectric properties of biomaterials in the far-infrared," Ph.D. thesis (University of Freiburg, 2005).
14. P. D. Cunningham, N. N. Valdes, F. A. Vallejo, M. L. Hayden, B. Polishak, X.-H. Zhou, J. Luo, A. K.-Y. Jen, J. C. Williams, and R. J. Twieg, "Broadband terahertz characterization of the refractive index and absorption of some important polymeric and organic electro-optic materials," J. Appl. Phys. **109**, 043505 (2011).
15. P. E. Powers, R. A. Alkuwari, J. W. Haus, K. Suizu, and H. Ito, "Terahertz generation with tandem seeded optical parametric generators," Opt. Lett. **30**, 640–642 (2005).
16. D. Grbovic and G. Karunasiri, "Fabrication of bi-material MEMS detector arrays for THz imaging," Proc. SPIE **7311**, 731108 (2009).
17. B. Scherger, M. Scheller, C. Jansen, M. Koch, and K. Wiesauer, "Terahertz lenses made by compression molding of micropowders," Appl. Opt. **50**, 2256–2262 (2011).
18. M. Wichmann, A. S. Mondol, N. Kocic, S. Lippert, T. Probst, M. Schwerdtfeger, S. Schumann, T. Hochrein, P. Heidemeyer, M. Bastian, G. Bastian, and M. Koch, "Terahertz plastic compound lenses," Appl. Opt. **52**, 4186–4191 (2013).
19. A. Siemion, A. Siemion, M. Makowski, M. Sypek, E. Hérault, F. Garet, and J.-L. Coutaz, "Off-axis metallic diffractive lens for terahertz beams," Opt. Lett. **36**, 1960–1962 (2011).
20. A. Siemion, A. Siemion, M. Makowski, J. Suszek, J. Bomba, A. Czerwiński, F. Garet, J.-L. Coutaz, and M. Sypek, "Diffractive paper lens for terahertz optics," Opt. Lett. **37**, 4320–4322 (2012).
21. B. Scherger, C. Jördens, and M. Koch, "Variable-focus terahertz lens," Opt. Express **19**, 4528–4535 (2011).
22. M. Wichmann, B. Scherger, S. Schumann, S. Lippert, M. Scheller, S. F. Busch, C. Jansen, and M. Koch, "Terahertz Brewster lenses," Opt. Express **19**, 25151–25160 (2011).
23. M. Janek, I. Bugár, D. Lorenc, V. Szöcs, D. Velič, and D. Chorvát, "Terahertz time-domain spectroscopy of selected layered silicates," Clays Clay Miner. **57**, 416–424 (2009).
24. M. Mizuno, K. Fukunaga, S. Saito, and I. Hosako, "Analysis of calcium carbonate for differentiating between pigments using terahertz spectroscopy," J. Eur. Opt. Soc. **4**, 09044 (2009).
25. M. Schwerdtfeger, E. Castro-Camus, K. Krügener, W. Viöl, and M. Koch, "Beating the wavelength limit: three-dimensional imaging of buried subwavelength fractures in sculpture and construction materials by terahertz time-domain reflection spectroscopy," Appl. Opt. **52**, 375–380 (2013).
26. A. Dreyhaupt, S. Winner, T. Dekorsy, and M. Helm, "High-intensity terahertz radiation from a microstructured large-area photoconductor," Appl. Phys. Lett. **86**, 121114 (2005).
27. G. Gallot and D. Grischkowsky, "Electro-optic detection of terahertz radiation," J. Opt. Soc. Am. B **16**, 1204–1212 (1999).
28. P. C. M. Planken, H.-K. Nienhuys, H. J. Bakker, and T. Wenckebach, "Measurement and calculation of the orientation dependence of terahertz pulse detection in ZnTe," J. Opt. Soc. Am. B **18**, 313–317 (2001).
29. Y. Kim, D.-S. Yee, M. Yi, and J. Ahn, "High-speed high-resolution terahertz spectrometers," J. Korean Phys. Soc. **56**, 255–261 (2010).
30. B. B. Hu and M. C. Nuss, "Imaging with terahertz waves," Opt. Lett. **20**, 1716–1718 (1995).
31. G. R. Fowles, *Introduction to Modern Optics*, 2nd ed. (Dover Publications, 1989).
32. W. Withayachumnankul, B. Ferguson, T. Rainsford, S. P. Mickan, and D. Abbott, "Material parameter extraction for terahertz time-domain spectroscopy using fixed-point iteration," Proc. SPIE **5840**, 221–231 (2005).
33. W. Withayachumnankul, B. Ferguson, T. Rainsford, S. P. Mickan, and D. Abbott, "Simple material parameter estimation via terahertz time-domain spectroscopy," Electron. Lett. **41**, 800–801 (2005).
34. A. C. Tennissen, *Nature of Earth Materials* (Prentice Hall, 1974).
35. B. K. Johnson, *Optics and Optical Instruments: An Introduction with Special Reference to Practical Applications* (Dover Publications, 1960).
36. E. Hecht, *Optics*, 4th ed. (Addison Wesley, 2002).